Sustainable Energy, Grids and Networks 44 (2025) 102055

Contents lists available at ScienceDirect

Sustainable Energy, Grids and Networks

journal homepage: www.elsevier.com/locate/segan

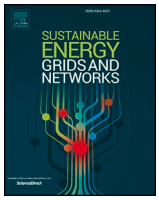

Short circuit analysis and voltage support needs in power systems with relevant share of inverter-based resources

Matteo Fresia *, Manuela Minetti, Andrea Bonfiglio, Renato Procopio

University of Genoa, Department of Electrical, Electronic, Telecommunications Engineering and Naval Architecture, Genoa, Italy

ARTICLE INFO

Keywords:
Inverter-based Resources
Short-Circuit
Faults
Optimization

ABSTRACT

The large-scale integration of Inverter-Based Resources (IBRs) in transmission networks introduces significant challenges for voltage regulation. This paper proposes a comprehensive methodology to evaluate the contribution of IBRs during fault conditions. The approach consists of two key steps: first, a quasi-analytical procedure is developed to calculate post-fault nodal voltages in networks with IBRs, avoiding the need for specialized power systems software and ensuring both accuracy and computational efficiency. Secondly, an optimization problem is designed to determine the optimal susceptance to be installed at network nodes, ensuring that local reactive power injection maintains nodal voltages within grid code requirements. The quasi-analytical method incorporates the specific Italian grid code requirements for IBR behaviour during faults. Results demonstrate that the proposed procedure achieves a maximum error of just 0.1 % compared to detailed simulations performed in DIgSILENT PowerFactory and highlight the inability of existing short-circuit calculation standards to accurately predict nodal voltages under the Italian grid code specifications. Furthermore, the optimization results are validated through simulations, confirming that the calculated susceptances effectively maintain nodal voltages within the prescribed limits. Overall, the proposed strategy provides an accurate modelling of IBR fault response in compliance with specific grid code requirements and an approach to determine the minimum reactive power support needed to maintain voltage during short-circuit events in networks with high IBR penetration. This procedure specifically addresses the limitations of general Short-Circuit (SC) standards for IBR modelling and offers a fast, practical tool for TSOs to evaluate voltage support needs in large transmission networks.

1. Introduction

Renewable Energy Sources (RESs) and Battery Energy Storage Systems (BESSs) are crucial to the energy transition. Due to their connection to the grid via power electronic converters, they do not ensure the same performances in frequency and voltage support of traditional Synchronous Generators (SGs): indeed, the massive integration of Inverter-Based Resources (IBRs) will lead to a reduction of the Short-Circuit (SC) power, the inertial response and the primary regulating energy of the system [1]. Focusing on voltage issues, a possible solution is represented by synchronous compensators, which, by the way, are able to provide inertial response too, limiting the rate of change of frequency of the system [2]. Nevertheless, synchronous compensators represent an expensive solution: consequently, the assessment of the voltage support capability of IBRs under SC conditions is fundamental for Transmission System Operators (TSOs).

If, on one hand, the calculation of the SC current contribution of SGs is well established [3], on the other hand, RESs and BESSs inverters' response to faults has been only recently analysed in depth. Due to their structure, they are able to sustain a limited overcurrent for few milliseconds, being possibly constrained to work in saturated conditions [4]. To determine the output current of inverters under fault conditions, it is necessary to consider the implemented current-limiting method, classified as direct or indirect: direct methods adjust current-reference or switch control signals to limit the output current, while indirect methods reduce the output current by modifying voltage or power reference signals within the inverter controls [4].

Standard IEC 60909 provides calculation methods for SC current contributions of both SGs and IBRs [5], stating that photovoltaic and wind turbine inverters can be modelled as current sources with infinite shunt impedance. In [6], a modelling approach to account three possible operational states of IBRS (unsaturated state, partially saturated state and fully saturated state), considering dedicated control schemes and

* Correspondence to: University of Genoa – Department of Electrical, Electronic, Telecommunications Engineering and Naval Architecture, Via Opera Pia 11a, Genoa 16145, Italy

E-mail address: matteo.fresia@edu.unige.it (M. Fresia).

https://doi.org/10.1016/j.segan.2025.102055
Received 6 August 2025; Received in revised form 21 October 2025; Accepted 10 November 2025
Available online 11 November 2025

Nomenclatures

AC	Alternating Current
AVR	Automatic Voltage Regulator
BESS	Battery Energy Storage System
CCP	Converter Connection Point
DC	Direct Current
HVDC	High Voltage Direct Current
IBR	Inverter-Based Resource
NLP	Non-Linear Programming
RES	Renewable Energy Source
SC	Short-Circuit
SG	Synchronous Generator
TSO	Transmission System Operator
WSCC	Western System Coordinating Council

power and voltage constraints, is proposed. The approach aims at assessing the possible equilibrium points that may emerge in a power system considering all the eventual current saturation states of the IBRs. In [7] the authors apply the procedure discussed in [6] to the analysis of distribution networks with IBRs during SC events, considering the presence of grid-following and grid-forming inverters that may operate simultaneously in different current saturation states. The proposed mathematical model is non-linear, thus relies on a numerical solver to be applied. The same authors extend the application field of the methodology in [8] and [9], where they focus on the evaluation of SC equilibrium points in a low-medium voltage photovoltaic field connected to the high voltage transmission network, analysing also the impact of fault location and medium voltage grid topology on the SC response of the system. From the methodological side, the model still relies on non-linear relations, making the usage of a numerical solver mandatory. Finally, the same authors developed in [10] a steady-state SC calculation solver for networks characterized by high penetration of IBRs, trying to overcome the need of detailed dynamic characterization: in particular, an extended Newton-Raphson solver is adopted, nevertheless not overcoming the non-linearity of model. Another methodology to evaluate the behaviour of IBRs during SCs is provided in [11], describing them either as voltage or current sources, depending on the entity of the considered fault. In [12], a methodology to find a network equivalent representing the steady-state SC response of a grid with large IBRs share is presented to overcome the limitations of classical Thevenin's equivalent; showing that this classical representation where IBRs are represented as a voltage dependent current source in parallel with a shunt impedance, produces less accurate results according to the increased share of IBRs installed in the examined network. Finally, the author of [13] highlights the need for a standardization of the response of IBRs under SC conditions. Moreover, the author highlights that SGs do not contribute with additional active current during faults (i.e., the SC current lags in quadrature the generator internal voltage) while IBRs may inject both active and reactive current during faults. Given that recent technical reports, like [14], allow the injection of active current by inverters, this means that, in scenarios with large RES penetration, the magnitude and the angle of SC currents could not follow the expected trend. Indeed, as highlighted in [15], even if the SC of IBRs contribution is limited with respect to the one of SGs, a considerable penetration RES and BESS power plants may change the magnitude and phase of SC current, thus making mandatory to include them in SC calculations.

In addition, the accurate calculation of post-fault voltages in transmission networks increasingly requires consideration of High Voltage Direct Current (HVDC) system behaviour during Direct Current (DC) side faults. Studies have shown that faults in modular multilevel converter-based multi terminal DC grids can lead to rapid discharge of capacitors, contributing significantly to fault currents and influencing adjacent Alternating Current (AC) system voltage [16]. Similarly, the interaction between converter control strategies and fault transients affects both DC and AC side dynamics in HVDC systems, necessitating detailed modelling of trigger angle variations of line commutated converters and AC current feeding of voltage source converters [17]. Furthermore, flexible DC grids introduce specific challenges, as the network topology play crucial roles in determining fault current contributions and subsequent voltage deviations [18]. The integration of renewable energy sources and HVDC links further complicates short-circuit analysis, as these elements alter traditional fault current characteristics and require advanced iterative solution methods to accurately capture post-fault voltage profiles [19]. Therefore, incorporating DC fault analysis is essential for comprehensive post-fault voltage assessment in modern hybrid AC/DC transmission systems.

From a methodology point of view, there are two characteristics that unite the approaches mentioned: *i)* they all rely on general standards (that may differ from the national TSO's prescriptions), thus requiring not negligible adjustments if one aims at applying them to analyse specified countries cases; *ii)* they all rely either on numerical solvers or on simulations through dedicated power systems software; *iii)* some of them focus just on low-medium voltage networks.

Thus, there is a research gap that consists in the lack of a method for SC calculation that adheres more to the prescription of TSOs and does not need any specialized (and thus commercial) solver to study fault conditions in transmission networks. In addition, the discussed studies limit themselves to the assessment of post-fault nodal voltage, without providing solutions to help TSOs in quantifying the additional resources that would be needed to support voltage in network strategic nodes.

To fill the existing research gap, this paper firstly proposes a procedure to calculate nodal voltages in transmission networks with large penetration of IBRs under fault conditions: the procedure is semi-analytical, since only the inversion of a matrix is needed, allowing for a precise and fast resolution procedure that does not rely on dedicated power systems software. Moreover, IBRs are modelled according to the prescription of the Italian Grid Code (i.e., Attachment A.79 [20]). Secondly, to estimate the voltage support needs during fault conditions, the paper proposes an optimization problem determining the reactive power to be injected at specified nodes of the grid to ensure that bus voltages variation during selected faults remains within a suitable range. Methodology effectiveness is evaluated by comparison with the results achieved via detailed RMS simulations, showing a good agreement between the proposed approach and the complete simulation. For the sake of complements, the proposed approach has been tested in two case studies: the 9-bus system introduced in [21], to allow an analytical and punctual assessment of the achieved results, and the IEEE 39-bus system [22] for a more significant validation in a realistic power grid. Both networks have been suitably modified to include a IBRs. Moreover, the nodal voltages obtained through the quasi-analytical procedure are furtherly compared with the ones obtained through the application of SC calculation standards usually implemented in several commercial tools: this comparison shows how the most common standards cannot comprehensively represent the fault behaviour required to IBRSs specifically by the Italian network code. To summarize, the novelty contribution of the proposed approach can be defined as: *(i)* the definition of a novel comprehensive methodology for the assessment of nodal voltage during fault conditions and *(ii)* the proposal of a strategy to assess the SC current needs to sustain nodal voltage while minimizing the reactive power injection into the network. Regarding *(i)*, the developed methodology is semi-analytical, involving just the inversion of a matrix as numerical calculation: differently from other available studies, this implies that the use of dedicated power system software to compute during-fault voltages can be overcome. Moreover, the procedure is general and can be applied to different national regulatory frameworks, requiring different supports by IBRs during faults. Concerning *(ii)*, the optimization problem is intended to support TSO in deciding the amount of additional devices to be inserted in IBR

dominated power systems to guarantee suitable condition during faults. The combination of the two methodologies is intended to provide a comprehensive tool allowing both to prevent disruptive operation of the system during faults, by assessing the additional resources to be installed to support voltage, and to assess the operating conditions of power systems during faults, overcoming dedicated power system software solutions.

The paper is structured as follows: Section 2 describes the quasi-analytical methodology and the subsequent optimization problem; Section 3 discloses and comments the results of the two procedures and Section 4 provides some conclusive remarks and proposes some possible future developments of the study.

2. Methodology

The mathematical model of the IBR, developed considering the requirements of the Italian grid code and used in the proposed methodology, is described in Section 2.1. Section 2.2 outlines the quasi-analytical procedure for assessing post-fault nodal voltages, while Section 2.3 defines the structure of the optimization problem aimed at minimizing the reactive power required at specific network nodes, identified by the TSO, to maintain voltage within acceptable limits. Specifically, the quasi-analytical procedure is designed to avoid reliance on specialized commercial power system software and to ensure computational efficiency for large-scale studies, allowing the identification of critical post-fault voltage values at network nodes. Subsequently, the optimization problem is employed to provide a systematic approach for determining the reactive power to be provided to restore the critical voltage values at strategic nodes (highlighted by the quasi-analytical procedure) within the TSO desired operational range.

2.1. Modelling of IBR according to Italian Grid Code requirements

The Italian grid code mandates that IBRs, such as the ones coupled with BESS, provide adequate voltage support during faults by adhering to the functional requirements described in Annex A.79 [22]. Note that Annex A.79 refers to the voltage value measured at the Converter Connection Point (CCP), where the inverter-based converter is connected through the connection reactance x_{IBR}, as illustrated in Fig. 1. Moreover, Annex A.79 refers to the quantities in the *dq* reference frame aligned with the voltage at the CCP.

Specifically, the grid code defines two possible operating conditions for the IBR, which will henceforth be referred to as normal and fault conditions. The normal operating condition occurs when the measured voltage at CCP is above the threshold V_{lim}, while the fault condition arises when the voltage falls below V_{lim}.

As detailed in [22], the IBR is required to operate in grid-forming mode under normal operating conditions. On the other hand, in fault conditions, the IBR is expected to actively contribute to voltage recovery by injecting reactive current proportional to the severity of the fault, also reducing, if needed, the active power output. Specifically, the d-q axis reference currents to be provided by the IBR are as follows:

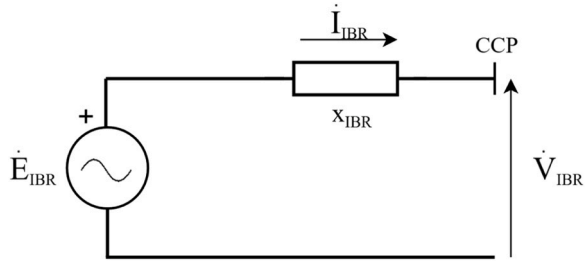

Fig. 1. Grid-Forming IBR equivalent scheme.

$$\begin{cases} I_d^* = 0 \\ I_q^* = K\cdot(V_{\text{lim}} - V_{IBR,d}) + \max(I_{q,PF}, 0) \end{cases} \tag{1}$$

where $I_{q,PF}$ represents the q-axis current value in the pre-fault condition and K is a proportional coefficient that can take a value from 0 to 5. According to (1), the reactive current provided by the IBR during the fault takes into account the pre-fault contribution only if the IBR was already supplying reactive power to the grid prior to the fault. The grid code requirements are implemented in the control scheme depicted in Fig. 2.

The grid-forming control, implemented under normal operating conditions, features a cascade configuration, with a voltage regulator providing the inner current regulator with suitable reference signals [23]. On the other hand, the current control, enabled under fault condition, provides the inner current regulator with the current reference signals (1).

To explicit a semi-analytical procedure for estimating the nodal voltages' phasors in a power grid, the requirements specified by the Italian grid code, originally defined in the d-q reference frame, must be reformulated as phasor equations to enable their integration into the proposed methodology.

Assuming instantaneous action of the voltage and control loops, the IBR in grid forming mode can be modelled as an ideal AC voltage source with a given magnitude V_{IBR} and phase δ_{IBR} and with low output reactance x_{IBR}, as represented in Fig. 1 [24].

Therefore, the IBR current $\dot{I}_{IBR}$ injected at the CCP under normal operation condition, can be determined as:

$$\dot{I}_{IBR} = \frac{\dot{E}_{IBR} - \dot{V}_{IBR}}{jx_{IBR}} \tag{2}$$

where $\dot{E}_{IBR}$ and $\dot{V}_{IBR}$ are the phasors of the equivalent voltage generator and the voltage at the CCP node, respectively.

Under fault conditions, according to the grid code requirements, the IBR is controlled as a current source that provides the current defined in (1). System (1) can be expressed in phasor form, as reported:

$$\dot{I}_{IBR} = K\cdot\left(V_{\text{lim}} - V_{IBR}\right)e^{j\left(\frac{\pi}{2}+\delta_{IBR}\right)} + \max\left\{I_{q,pf}e^{j\left(\frac{\pi}{2}+\delta_{IBR}\right)}, 0\right\} \tag{3}$$

where δ_{IBR} is the phase of the voltage at CCP. As the non-linearity of the second term in (3) makes the problem analytically intractable, one can neglect the contribution related to the pre-fault component. Indeed, the fact that the parameter K can lay in a (quite wide) range gives the opportunity of compensating this missing contribution with a different choice of K. An additional aspect to consider when determining the coefficient K is the saturation of the inverter under fault conditions. Indicating with I_{lim} the maximum current that the IBR can provide based on its capability, the magnitude of the IBR current, in the worst-case scenario (i.e., when a 3-phase fault occurs at the CCP node), should be limited to:

$$I_{IBR} \le K\cdot(V_{\text{lim}} - V_{IBR}) \le K\cdot V_{\text{lim}} \le I_{\text{lim}} \tag{4}$$

Therefore, one has that K should be chosen s.t.:

$$0 \le K \le \min\left(\frac{I_{\text{lim}}}{V_{\text{lim}}}, 5\right) \tag{5}$$

In conclusion, in the following semi-analytical procedure, the compliance to the grid code requirements will be implemented as follows:

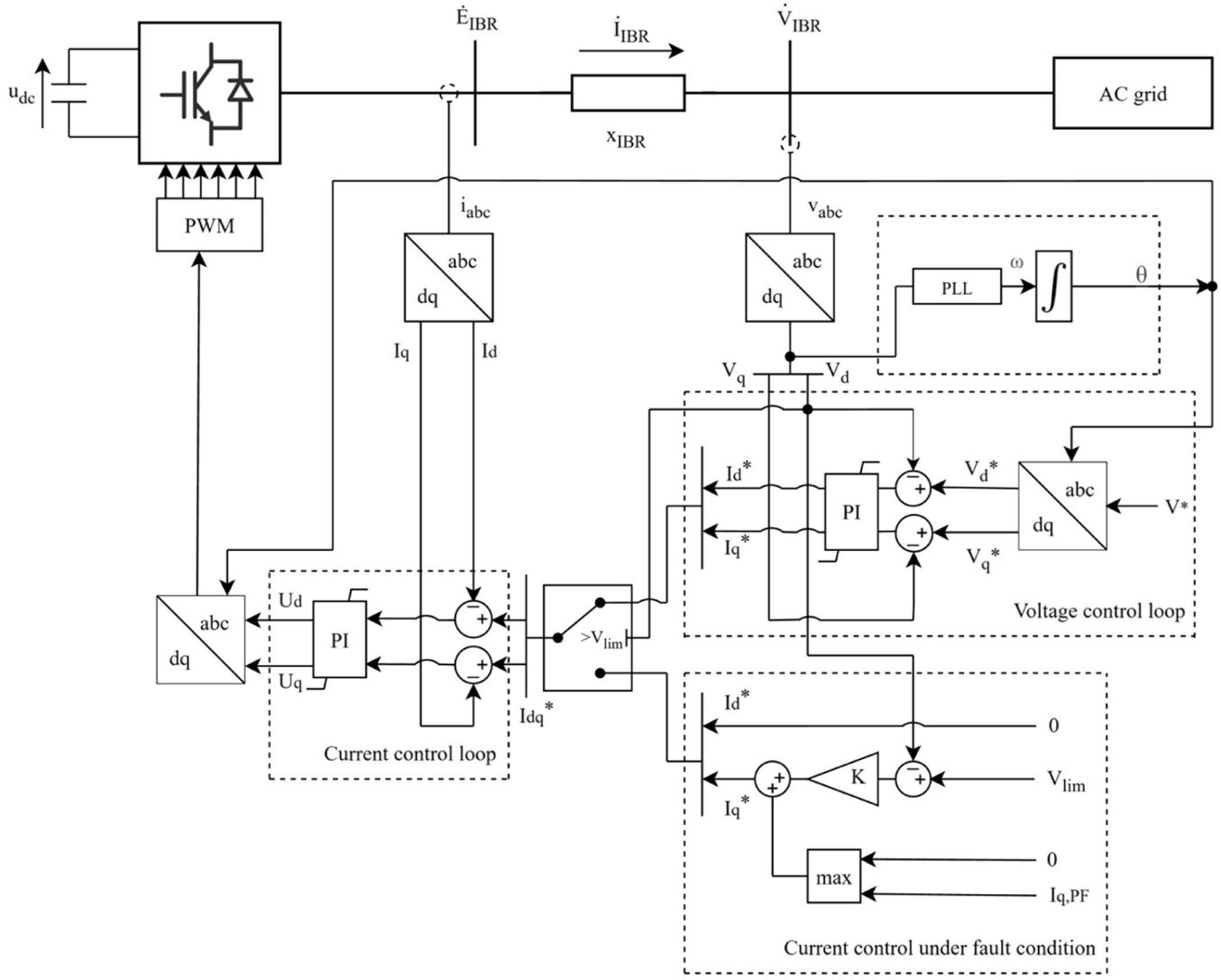

Fig. 2. Control scheme of IBRs.

$$\dot{I}_{IBR} = \begin{cases} \dfrac{\dot{E}_{IBR} - \dot{V}_{IBR}}{jx_{IBR}} & if \;\; V_{IBR} \geq V_{\lim} \\ K \cdot \left(V_{\lim} - V_{IBR} \right) e^{j\left(\frac{\pi}{2} + \delta_{IBR}\right)} & else \end{cases} \tag{6}$$

with K belonging to the range defined in (5). Note that the approximation of neglecting the eventual pre-fault positive quadrature axis current is just posed here to accomplish a semi-analytical solution: the full model of the behaviour of IBRs under faults, as prescribed by the grid code, is instead implemented in the complete simulation that will be presented as benchmark to validate the proposed approach.

2.2. Semi-analytical procedure for short circuit nodal voltage calculation

Given a network, the current injection $\dot{I}_i$ at bus i is given by:

$$\dot{I}_i = \sum_{k=1}^{N} \dot{Y}_{ik} \cdot \dot{V}_k \qquad \forall i = 1, \ldots, N \tag{7}$$

where $\dot{Y}_{ik}$ is the *(i,k)*-th element of the network admittance matrix and $\dot{V}_k$ is the voltage at bus k, where N is the number of busses of the considered network.

To perform the fault analysis, it is common to model loads as constant admittances, whose value is obtained starting from the active and reactive power absorptions and from the local voltage in pre-perturbation conditions, as shown in:

$$\dot{Y}_i = \frac{P_i - jQ_i}{V_{LF,i}^2} \qquad \forall i = 1, \ldots, N^L \tag{8}$$

where $\dot{Y}_i$ is the equivalent load admittance, P_i and Q_i are the active and reactive power absorbed by the load at bus i, $V_{LF,i}$ is the pre-perturbation voltage amplitude at bus i and N^L is the number of load busses.

SGs current injection is characterized as follows:

$$\dot{I}_i = \frac{\dot{E}_{0,i} - \dot{V}_i}{jx_i^{''}} \qquad \forall i = N^L + 1, \ldots, N^L + N^{SG} \tag{9}$$

where $\dot{E}_{0,i}$ is the subtransient electromotive force and $x_i^{''}$ is the subtransient reactance of the i-th SG, where N^{SG} is the number of SG busses. A second-order SG model is adopted in (9), since it is coherent with the time horizon of the analysis, aimed at evaluating the current injection immediately after the fault occurrence [25].

IBRs behaviour under fault is modelled considering the prescriptions of grid codes, adapting the formulation presented in (6). In formulas:

$$\dot{I}_{IBR,i} = \begin{cases} \dfrac{\dot{E}_{IBR,i} - \dot{V}_i}{jx_{IBR,i}} & if\ V_i < V_{\lim} \\ K \cdot \left(V_{\lim} - V_i\right) e^{j\left(\frac{\pi}{2}+\delta_i\right)} & else \end{cases} \quad \forall i = N^L + N^{SG} + 1, \ldots, N^L + N^{SG} + N^{IBR} \tag{10}$$

where $\dot{E}_{IBR,i}$ is the voltage of the equivalent voltage source of the i-th inverter, $\dot{V}_i$ is the voltage of at the CCP busbar of the i-th inverter (indicated in Section 2.1 as $\dot{V}_{IBR,i}$), $x_{IBR,i}$ is the connection reactance of the i-th inverter and δ_i is the phase of $\dot{V}_i$, where N^{IBR} is the number of IBRs in the considered network.

Since loads and SGs are characterized through linear equations, it is possible to define a linear set of $(N^L + N^{SG})$ equations with $(N^L + N^{SG})$ unknows that allows to find the voltages at load and SG network busbars as functions of the voltages at IBRs network busbars.

For load busbars, one can write:

$$\dot{Y}_i \dot{V}_i + \dot{Y}_{g,i} \dot{V}_i + \sum_{k=1}^{N^L+N^{SG}} \dot{Y}_{ik} \dot{V}_k + \sum_{k=N^L+N^{SG}+1}^{N} \dot{Y}_{ik} \dot{V}_k = 0 \quad \forall i = 1, \ldots, N^L \tag{11}$$

where $\dot{Y}_{g,i}$ is the fault admittance at bus i (equal to 0 if the fault is not located at bus i). Eq. (11) can be rewritten as:

$$\sum_{k=1}^{N^L+N^{SG}} \left[-\dot{Y}_{ik} - \left(\dot{Y}_i + \dot{Y}_{g,k}\right) \cdot \delta_{ik} \right] \cdot \dot{V}_k = \sum_{k=N^L+N^{SG}+1}^{N} \dot{Y}_{ik} \dot{V}_k \quad \forall i = 1, \ldots, N^L \tag{12}$$

where δ_{ik} is Kronecker's delta. Eq. (12) can be furtherly rearranged and expressed in matrix form as:

$$[A_L] \times \begin{bmatrix} \left[\dot{V}_L\right] \\ \left[\dot{V}_{SG}\right] \end{bmatrix} = \left[\dot{Y}_{L,IBR}\right] \times \left[\dot{V}_{IBR}\right] \tag{13}$$

in which $\left[\dot{V}_L\right]$, $\left[\dot{V}_{IBR}\right]$ and $\left[\dot{V}_{SG}\right]$ are column vectors collecting the voltages at load, IBR and SGs busbars respectively and $\left[\dot{Y}_{L,IBR}\right]$ is the partition of the network admittance matrix correlating load and IBR busbars (i.e. N^L rows and N^{IBR} columns), having defined the generic element of matrix $[A_L]$ as:

$$\begin{aligned} A_{L_{ik}} &= -\dot{Y}_{ik} - \left(\dot{Y}_i + \dot{Y}_{g,k}\right) \cdot \delta_{ik} \\ \forall i = 1, \ldots, N^L,\ \forall k &= 1, \ldots, N^L + N^{SG} \end{aligned} \tag{14}$$

Similarly, for SGs busbars, the describing equation is:

$$\frac{\dot{E}_{0,i} - \dot{V}_i}{jx_i''} - \dot{Y}_{g,i} \dot{V}_i = \sum_{k=1}^{N^L+N^{SG}} \dot{Y}_{ik} \dot{V}_k + \sum_{k=N^L+N^{SG}+1}^{N} \dot{Y}_{ik} \dot{V}_k \quad \forall i = N^L + 1, \ldots, N^L + N^{SG} \tag{15}$$

Eq. (15) can be rearranged as:

$$\sum_{k=1}^{N^L+N^{SG}} \left[-\dot{Y}_{ik} + \left(\frac{j}{x_k''} - \dot{Y}_{g,k}\right) \cdot \delta_{ik} \right] \cdot \dot{V}_k = \sum_{k=N_c+N_s+1}^{N} \dot{Y}_{ik} \dot{V}_k + \frac{j}{x_i''} \dot{E}_{0,i} \quad \forall i = N^L + 1, \ldots, N^L + N^{SG} \tag{16}$$

which can be rewritten in matrix form as:

$$[A_{SG}] \times \begin{bmatrix} \left[\dot{V}_L\right] \\ \left[\dot{V}_{SG}\right] \end{bmatrix} = \left[\dot{Y}_{SG,IBR}\right] \times \left[\dot{V}_{IBR}\right] + j \left[\frac{\dot{E}_0}{x''}\right] \tag{17}$$

in which $\left[\dot{Y}_{SG,IBR}\right]$ is the partition of the network admittance matrix correlating SG and IBR busbars (i.e. N^{SG} rows and N^{IBR} columns), $\left[\frac{\dot{E}_0}{x''}\right]$ is a column vector collecting the ratios between the electromotive forces of SGs and their subtransient reactance, having defined the generic element of matrix $[A_{SG}]$ as:

$$A_{SG_{ik}} = -\dot{Y}_{ik} + \left(\frac{j}{x_k''} - \dot{Y}_{g,k}\right) \cdot \delta_{ik} \quad \forall i = N^L + 1, \ldots, N^L + N^{SG},\ \forall k = 1, \ldots, N^L + N^{SG} \tag{18}$$

The coupled resolution of (13) and (17) leads to the expression of the load and the SG busbar voltages as functions of the voltages at the CCP busbars of the IBRs, as follows:

$$\begin{bmatrix} \left[\dot{V}_L\right] \\ \left[\dot{V}_{SG}\right] \end{bmatrix} = \begin{bmatrix} [A_L] \\ [A_{SG}] \end{bmatrix}^{-1} \times \begin{bmatrix} \left[\dot{Y}_{L,IBR}\right] \\ \left[\dot{Y}_{SG,IBR}\right] \end{bmatrix} \times \left[\dot{V}_{IBR}\right] + j \begin{bmatrix} [A_L] \\ [A_{SG}] \end{bmatrix}^{-1} \times \begin{bmatrix} [0]_{N^L \times 1} \\ \left[\frac{\dot{E}_0}{x''}\right]_{N^{SG} \times 1} \end{bmatrix} \tag{19}$$

Eq. (19) can be rewritten in element-wise formulation, as in (20) for load busbars and for SG busbars.

$$\dot{V}_i = \sum_{k=N_L+N_{SG}+1}^{N} \Psi_{i,k-N_L-N_{SG}} \dot{V}_k + j \sum_{k=1}^{N_L+N_{SG}} \Lambda_{ik} \Phi_k \quad \forall i = 1, \ldots, N^L + N^{SG} \tag{20}$$

having defined:

$$[\Lambda] = \begin{bmatrix} [A_L] \\ [A_{SG}] \end{bmatrix}^{-1} \tag{21}$$

$$[\Psi] = [\Lambda] \times \begin{bmatrix} \left[\dot{Y}_{L,IBR}\right] \\ \left[\dot{Y}_{SG,IBR}\right] \end{bmatrix} \tag{22}$$

$$[\Phi] = \begin{bmatrix} [0]_{N^L \times 1} \\ \left[\frac{\dot{E}_0}{x''}\right]_{N^{SG} \times 1} \end{bmatrix} \tag{23}$$

Specifically, the k-th element of matrix $[\Phi]$ can be defined as:

$$\Phi_k = \begin{cases} 0 & \forall k = 1, \ldots, N^L \\ \dfrac{\dot{E}_{0,k}}{x_k''} & \forall k = N^L + 1, \ldots, N^L + N^{SG} \end{cases} \tag{24}$$

Following a similar approach, voltages at CCP busbars can be found through Kirchoff's current law at relevant busbars as:

$$\Omega_i - \dot{Y}_{g,i} \dot{V}_i = \sum_{k=1}^{N^L+N^{SG}} \dot{Y}_{ik} \dot{V}_k + \sum_{k=N^L+N^{SG}+1}^{N} \dot{Y}_{ik} \dot{V}_k \quad \forall i = N^L + N^{SG} + 1, \ldots, N \tag{25}$$

in which the voltages appearing in the first sum of the right-hand side of the equality represent the voltages at load and SG busbars, that are in turn function of the CCP busbar voltages of IBRs as indicated by Eq. (20), while Ω_i describes the IBR current injection according to the CCP voltage, as required by the Italian grid code [22]. In formulas, Ω_i can be expressed as:

$$\Omega_i = \begin{cases} \dfrac{\dot{E}_{IBR,i} - \dot{V}_i}{jx_{IBR,i}} & if\ V_i \geq V_{\lim} \\ K \cdot \left(V_{\lim} e^{j\frac{\pi}{2}} - V_i e^{j\left(\frac{\pi}{2}+\delta_i\right)}\right) & else \end{cases} \tag{26}$$

where δ_i is the phase of $\dot{V}_i$ and the second equation is derived from (10), that would be in principle non-linear: thus, it is purposely modified in order to provide a linear correlation describing the behaviour of IBRs in undervoltage conditions.

Finally, substituting (20) in (25), it is possible to find the post-fault voltages at CCP busbars, that could be in turn substituted into (26) to find the voltages at load and SG busbars.

As first attempt, the first of (26) is used to characterize the current injection of IBRs. If, after substituting (20) in (25), for the i^*-th IBR node the CCP voltage is in module smaller than V_{lim}, the set of Eqs. (20)-(25) is again solved by applying the second of (26) to model the response of the i^*-th IBR.

The if-condition appearing in (26) does not introduce non-linearity into the system, as the set of equations is first solved by modelling the IBRs in the network as working in grid-forming mode (i.e., using the first expression in (26)). Then, the set of equations is again solved only if the voltage at a node i^*, to which the i^*-th IBR is connected, falls below the threshold V_{lim}: in this case, the i^*-th IBR behaviour in fault conditions is defined by the second of (26).

The analytical procedure is iterated until all the IBRs follow the prescriptions of grid codes, either working in GFo mode or in fault-mode. Moreover, in accordance with the grid code, an IBR that exits the GFo operating mode maintains its fault-mode functionality even if

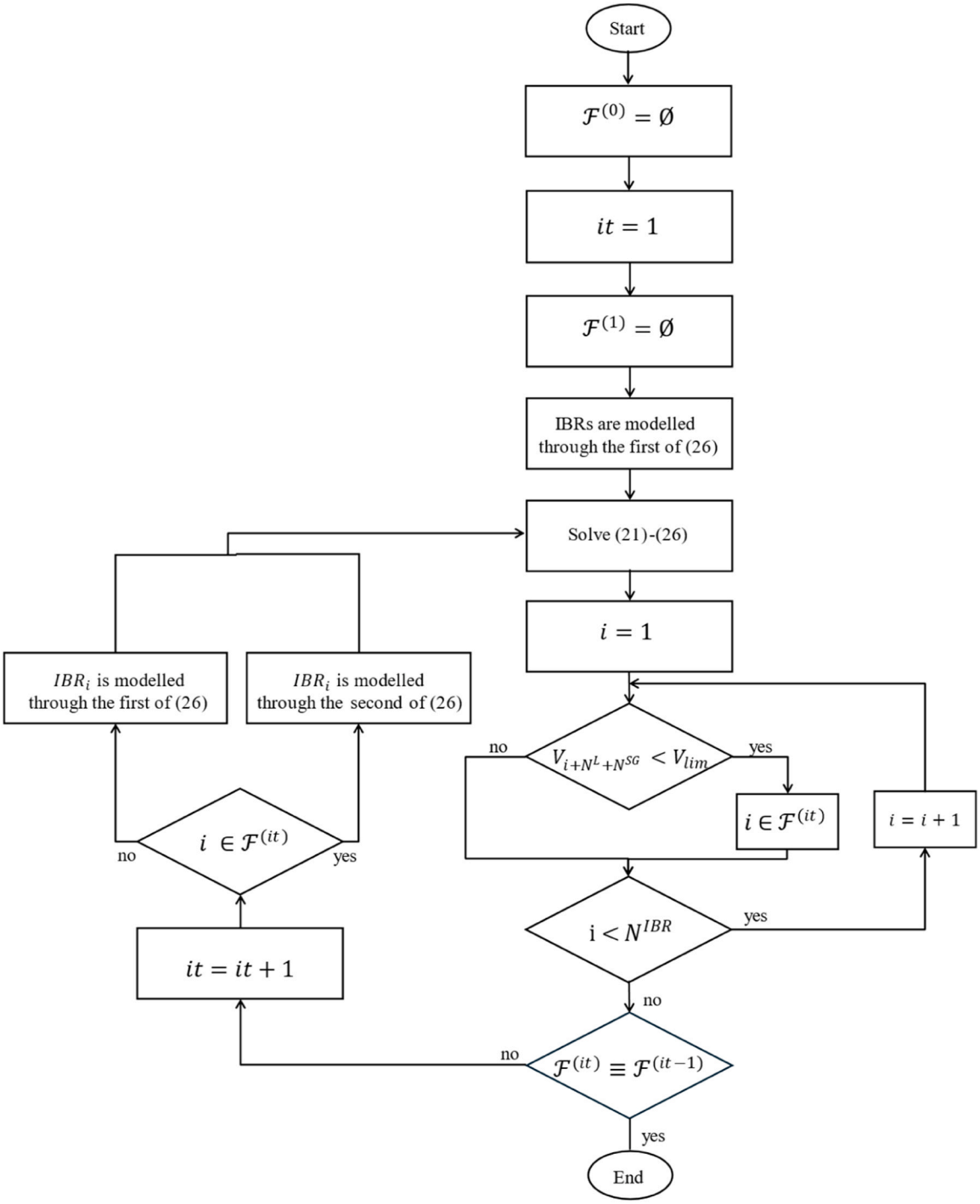

Fig. 3. Flowchart for the application of the semi-analytical procedure.

the voltage at its connection node subsequently exceeds $V_{\lim}$. For clarity, the flowchart illustrating the application of the semi-analytical procedure is presented in Fig. 3, where *it* denotes the iteration index, and $\mathscr{F}$ represents the set of nodes connected to IBRs with voltage values below $V_{\lim}$.

2.3. Optimal susceptance amount to be connected at given nodes in the network to support voltage during short circuit

Suppose now that, after a short circuit, the nodal voltages are too low. The question that can arise at this point is relevant to which actions the TSO can take to support them. In what follows, a methodology is provided, aimed at finding the optimal values of susceptances to be connected at given network nodes (from now on "strategic nodes") to keep voltages within predefined admissible ranges. The methodology consists of an optimization problem that ensures the minimization of the reactive power circulation in the system (minimizing the additional injected reactive power). Note that: *i)* the choice of the strategic nodes is beyond the scope of the work and so, in what follows, one will assume these nodes to be known and *ii)* the proposed is technologically agnostic, since it does not consider a specific technology for the provision of the additional reactive power.

The optimization problem is modelled as a Non-Linear Programming (NLP) problem.

The objective function to be minimized is:

$$Obj = \alpha \cdot \frac{\sum_{i\in\Gamma}\left(B_{add,i}\cdot V_{POST,i}^2\right)}{Q_{ref}} + (1-\alpha)\cdot\frac{\sum_{i\in\Gamma}\left(V_{POST,i}-V_{ref,i}\right)^2}{\Delta V_{ref}} \tag{27}$$

where Γ denotes the set of network strategic nodes, $B_{add,i}$ and $V_{POST,i}$ are two sets of continuous decision variables, representing respectively the additional susceptance to be added at the *i*-th strategic node and its post-fault voltage amplitude, and $V_{ref,i}$ represents the reference voltage at the *i*-th strategic node, that may be the pre-fault one or the nominal one. The adopted approach is multi-objective; thus coefficient α, varying between 0 and 1, is employed to establish a Pareto front analysis. To ensure an effective optimization, the two terms of the objective function have to be normalised respectively on Q_{ref} and ΔV_{ref}, that are respectively determined as the sum of the nodal reactive power injection in relevant the worst scenario (i.e., when $\alpha = 0$) and as the sum of the quadratic voltage difference in relevant the worst scenario (i.e., when $\alpha = 1$).

The first set of constraints has the aim of defining the admittable interval for voltage modules at SG and IBR busbars:

$$V_{\min} \le V_i \le V_{\max} \quad \forall i \in \Gamma \tag{28}$$

where $V_{\min}$ and $V_{\max}$ represent the lower and upper bounds for voltage modules.

Two further set of constraints are needed to technically constrain the installation of nodal susceptance and to prevent its installation at non-strategic nodes.

$$B_{add,i} \ge 0 \quad \forall i \in \Gamma \tag{29}$$

$$B_{add,i} = 0 \quad \forall i \notin \Gamma \tag{30}$$

Regarding the modelling of the three categories of busbars (loads, SGs and IBRs), three sets of dedicated constraints are formulated. A first set of constraints describes the relation between current injections and nodal voltages at load busbars. In formulas:

$$-\dot{Y}_i\cdot\dot{V}_{POST,i} - jB_{add,i}\cdot\dot{V}_{POST,i} - \sum_{k=1}^{N}\dot{Y}_{ik}\cdot\dot{V}_{POST,k} = 0 \quad \forall i = 1,\dots,N^L \tag{31}$$

Regarding SG busbars, the model proposed in (9) is adapted considering the impact that a possibly-added susceptance may have on local voltage. In formulas:

$$\frac{\dot{E}_{0,i}-\dot{V}_{POST,i}}{j\dot{x}_i} - jB_{add,i}\cdot\dot{V}_{POST,i} - \sum_{k=1}^{N}\dot{Y}_{ik}\cdot\dot{V}_{POST,k} = 0 \quad \forall i = N^L+1,\dots,N^L+N^{SG} \tag{32}$$

Similarly, for what concerns IBR busbars, the formulation presented in (25) is adapted, considering the possible installation of additional susceptance. In formulas:

$$\frac{\dot{E}_{IBR,i}-\dot{V}_{POST,i}}{j\dot{x}_{IBR,i}} - jB_{add,i}\cdot\dot{V}_{POST,i} - \sum_{k=1}^{N}\dot{Y}_{ik}\cdot\dot{V}_{POST,k} = 0 \quad \forall i = N^L+N^{SG}+1,\dots,N \tag{33}$$

Note that (33) holds if one chooses $V_{\min} > V_{\lim}$. In this way the conditions to apply the second of (10) never occur. The physical meaning of such choice is that the installation of additional susceptance is aimed at preventing the occurrence of significant undervoltage conditions that would activate the schemes required by grid codes. In this way, IBRs are able to work in Grid-Forming mode.

3. Numerical test and validation

The procedure to calculate nodal voltages in networks with large penetration of IBRs and the optimization procedure proposed to define the optimal amount of reactive power to be provided at the strategical nodes to keep nodal voltages at acceptable levels even under SC faults are tested on two standard networks.

The first test network used for validation is the 9-Bus system, a simplified representation of the Western System Coordinating Council (WSCC) [26]. The second network is the 39-Bus New England System, which covers a broader geographic area, shown in [27]. Both networks were implemented in the DIgSILENT PowerFactory environment and include two IBRs.

Preliminarily to the comment of the results, it has to be highlighted that the quasi-analytical procedure determines the voltage values "immediately after the contingency". Therefore, its results are compared with the ones obtained at the time instant at which short circuit current is provided by IBRs.

To assess the performances of the optimization algorithm, V_{min} and V_{max} are set to 0.85 p.u. and 1.05 p.u. and it is supposed that the set of strategic nodes coincides with the set of generation (IBR and SG) nodes. Moreover, as the optimization problem does not include the identification of the most appropriate technology, the design of the corresponding control system and the technological details of its implementation are beyond the scope of the work. For this reason, in the proposed validation, the delay time between the fault time instant and the one in which the additional susceptances are installed is neglected, as it is inherently dependent on the adopted technology.

The optimization problem has been implemented in Matlab-Yalmip [28] environment and solved through the *ipopt* library solver [29].

3.1. Power factory modelling and validation

To demonstrate the effectiveness of the proposed procedures, the WSCC 9-bus and 39-Bus New England System networks were implemented in PowerFactory using a more detailed representation of the technologies compared to the model described in the quasi-analytical procedure. Loads have constant active and reactive power demand in the load flow calculation, while during the RMS simulation are modelled as constant impedances. The SGs are modelled using the standard RMS dynamic model equipped with an Automatic Voltage Regulator (AVR) and a governor [30]. AVRs used for the SGs in the WSCC 9-bus and in the 39 Bus New England are rotating excitation system of IEEE Type 1 and the parameters' values are modified respectively according to [21,27]. The IBRs are modelled as two-level PWM converters controlled as described in Fig. 2. In compliance with the Italian grid code, the voltage

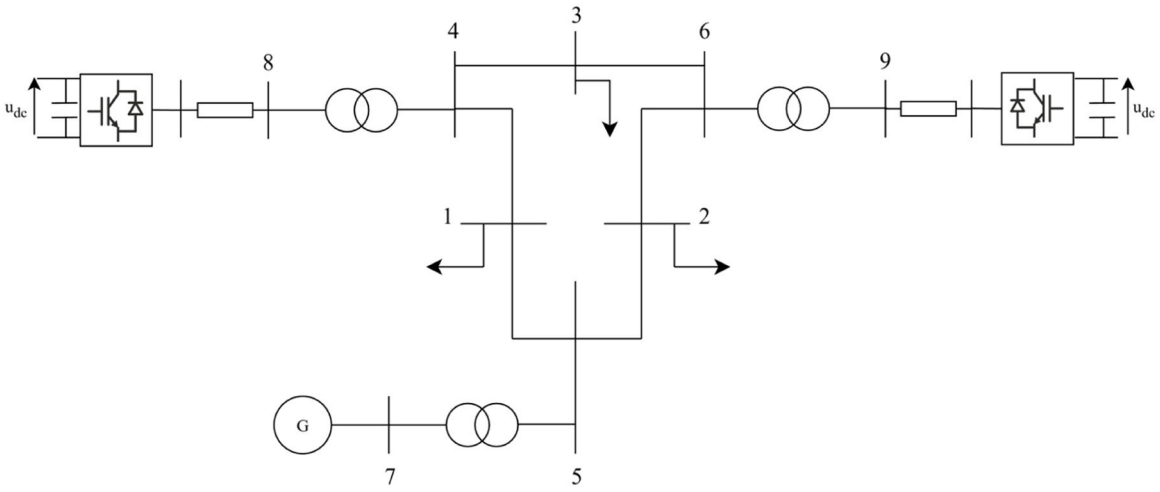

Fig. 4. WSCC 9-Bus Network implemented in DIgSILENT PowerFactory.

limit V_{lim} is 0.85 p.u. and the value of the control parameter K was set for all IBRs to the maximum value of the admissible range (5), adopting a conservative approach.

3.2. WSCC 9-bus test case

The reference WSCC 9-bus Test Case [26] is modified for the purpose of this paper, substituting the SGs connected to nodes 8 and 9 with two IBRs, as depicted in Fig. 4. This benchmark network includes three voltage levels: 16.5 kV for the SG, 20 kV for the IBRs and 230 kV for the high voltage section of the network. The SG rated power is equal to 247.5 MVA, while both IBRs have a rating of 33.33 MVA. The IBRs are connected to the network through a connection reactance, whose value is set to 0.05 p.u. on the local base. All other parameters of the system can be found in [31], and SG data are defined in [32].

The pre-contingency load flow assignments for IBRs, SG and loads are listed in Table 1. Nodes 1, 2 and 3 are load busbars, nodes 4, 5 and 6 are transit busbars and nodes 7, 8 and 9 are generation busbars. The considered contingency is a three-phase zero-impedance symmetrical fault occurring at node 2 after 0.1 s from the beginning of the simulation.

Table 2 presents the amplitude and phase values of the voltages at the generation nodes obtained using the proposed quasi-analytical procedure and the reference RMS simulation, along with the voltage amplitude percentual errors.

The dynamic responses of the inverters, in terms of voltage and power, is characterized by the rapid reaction of the IBR regulators, as shown in Fig. 5 and Fig. 6. For both inverters, since the CCP voltage is below 0.85 p.u., the current control under fault conditions, illustrated in Fig. 2, is activated.

Moreover, the analytical procedure results are compared with the ones obtained in DIgSILENT PowerFactory through the application of the most used standards for SC calculations: the German standard VDE 0102, the international standard IEC 60909 for calculating SC currents in three-phase AC systems, the American standard ANSI and the Complete standard. Results shown in Table 3 highlight that the standards for SC calculations are not effective when the IBRs in the network are controlled to meet the requirements of the Italian grid code. VDE 0102 and IEC 60909 model IBRs as current sources, while ANSI models IBRs as equivalent SGs and Complete as voltage sources. For more specific details, see [33] and references therein.

The optimization problem presented in Section 2.3. was solved for the described fault scenario. The optimal values of susceptances were inserted in the model developed in PowerFactory and the voltage values obtained from the simulation are reported in Table 4. Given the formulation of the optimization problem that aims at the minimization of the reactive power injection at the strategic nodes, the optimal solution is found for a condition in which the local voltage modules are kept at the minimum feasible value.

In order to analyse the trade-off between minimisation of the reac-

Table 1
WSSC 9-bus network – Load Flow assignments.

	LF type	Active power [MW]	Reactive power [MVAR]	Voltage module [p.u.]	Voltage phase [deg]
Bus 1	PQ	125	50	-	-
Bus 2	PQ	90	30	-	-
Bus 3	PQ	100	35	-	-
Bus 4	PQ	0	0	-	-
Bus 5	PQ	0	0	-	-
Bus 6	PQ	0	0	-	-
Bus 7	Slack	-	-	1.04	0
Bus 8	PV	10	-	1	-
Bus 9	PV	10	-	1	-

Table 2
WSSC 9-bus network – Post-fault voltages.

Voltage	Proposed method	Reference	Percentage error in voltage amplitude
$\dot{V}_7$	$0.7096\angle 8.39$	$0.7092\angle 8.38^\circ$	+0.06%
$\dot{V}_8$	$0.3054\angle -15.38$	$0.3034\angle -15.42^\circ$	+0.66%
$\dot{V}_9$	$0.1911\angle -22.81$	$0.1902\angle -22.81^\circ$	+0.47%

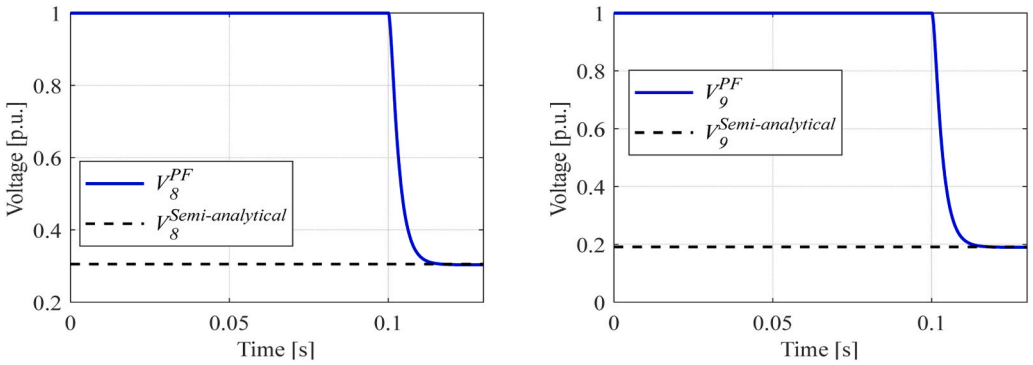

Fig. 5. Voltage magnitude of IBRs connected to nodes 8 and 9.

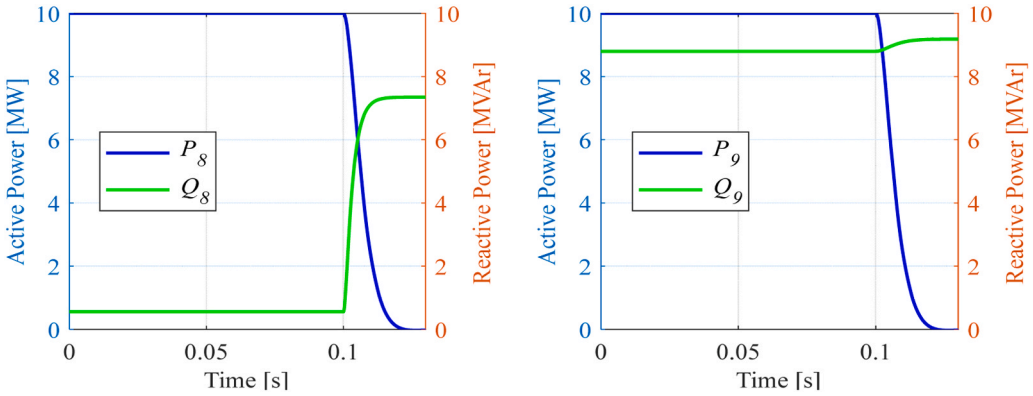

Fig. 6. Active and reactive power injections of IBRs connected to nodes 8 and 9.

Table 3
WSCC 9-bus network – Post-fault voltages – Comparison with other standards.

Voltage	Proposed method	VDE 0102	IEC 60909	ANSI	Complete
V_7	0.7096	0.6794	0.6794	0.6322	0.8331
V_8	0.3054	0.2228	0.2228	0.2976	0.3512
V_9	0.1911	0.1117	0.1117	0.1856	0.2123

tive power injection at strategic nodes and the voltage drop at those nodes, a Pareto analysis has been developed, varying the coefficient α between 0 and 1 with a step of 0.1. To this purpose, the reference voltages $V_{ref,i}$ for strategic nodes have been considered equal to the rated voltage (i.e., $V_{ref,i} = 1$). The voltage modules at strategic nodes when varying α are reported in Table 5, while nodal reactive power injection results are reported in Table 6.

Considering $\alpha = 0$, it is possible to keep all the voltages at the strategic nodes at the rated value, with the penalization of the reactive power injection that reaches the maximum values. Increasing the Pareto weight coefficient, nodal voltages progressively detach from rated values, down to the scenario with $\alpha = 1$, in which the voltages reach the minimum allowable value: on the other hand, the reactive power injection is minimised, with a reduction around −60% with respect to the first scenario.

The trade-off between the two objectives is well represented by the Pareto front shown in Fig. 7, in which Obj_1 and Obj_2 are respectively the first and second term of (27). For low values of α, between 0 and 0.2, it is possible to keep the strategic nodes at almost the rated value while reducing the local additional susceptances and the relevant reactive power injection: beyond values of $\alpha = 0.3$, the trade-off between the two objectives becomes more evident, reaching the apex in case of $\alpha = 0.9$ and $\alpha = 1$, with the nodal voltage deviation reaching the maximum value.

Table 4
WSCC 9-bus network – Optimization results.

Bus	$Q_{add}[MVAr]$	$B_{add}[\mu S]$	$\dot{V}$	
			Proposed method	Reference
7	179.670	913,450	$\angle 5.484°$	$0.8500\angle 5.372°$
8	38.180	132,101	$\angle -23.53°$	$\angle -23.32°$
9	186.1	643,967	$\angle -25.40°$	$\angle -24.98°$

3.3. New England 39-bus test case

The proposed procedure has been tested also on the 39-Bus New England System Test Case shown in [27]. This benchmark network consists of 2 IBRs, 8 SGs, 19 loads, 34 transmission lines and 12 transformers, as represented in Fig. 8.

Notably, one of the SGs (Gen1) is not a traditional rotating machine but represents the interconnection with Canada and the rest of the USA. As such, it is connected directly at the high-voltage level and operates without any type of controller. The network features four voltage levels: 138 kV for bus 12, 230 kV for bus 20, 16.5 kV for SG busses (bus 30 to bus 36), 20 kV for IBRs and 345 kV for the other busses. The 2 IBRs have been installed in place of the generators at busbars 38 and 39, while the loads at nodes 30 and 31 have been removed. Details about the generators, transmission lines, and transformers are provided in [27]. Additionally, the load flow assignments for the loads are detailed in [27], while those for the generators and IBRs appear in Table 7. IBRs ratings are considered equal to 100 MVA and the connection reactances are set equal to 0.05 p.u. on the local base.

A three-phase symmetrical fault was assumed to occur at node 20, 0.1 s after the beginning of the simulation. Table 8 presents the voltage values at generation busses obtained using the quasi-analytical procedure, alongside those derived from the simulation in PowerFactory. The maximum percentage difference between the voltage magnitudes

Table 5
WSCC 9-bus network – Pareto analysis of nodal voltages.

[p.u.]	$\alpha = 0$	$\alpha = 0.1$	$\alpha = 0.2$	$\alpha = 0.3$	$\alpha = 0.4$	$\alpha = 0.5$	$\alpha = 0.6$	$\alpha = 0.7$	$\alpha = 0.8$	$\alpha = 0.9$	$\alpha = 1$
Bus 7	1.000	0.993	0.984	0.972	0.957	0.936	0.905	0.855	0.850	0.850	0.850
Bus 8	1.000	0.997	0.993	0.988	0.981	0.971	0.956	0.931	0.884	0.850	0.850
Bus 9	1.000	0.996	0.990	0.983	0.973	0.960	0.941	0.908	0.850	0.850	0.850

Table 6
WSCC 9-bus network – Pareto analysis of nodal reactive power injections.

[MVAR]	$\alpha = 0$	$\alpha = 0.1$	$\alpha = 0.2$	$\alpha = 0.3$	$\alpha = 0.4$	$\alpha = 0.5$	$\alpha = 0.6$	$\alpha = 0.7$	$\alpha = 0.8$	$\alpha = 0.9$	$\alpha = 1$
Bus 7	495.33	477.73	456.08	428.83	393.52	346.11	279.47	180.58	176.54	179.68	179.68
Bus 8	172.00	169.54	166.46	162.50	157.23	149.85	138.81	120.49	76.44	38.18	38.18
Bus 9	375.79	369.34	361.33	351.15	337.77	319.40	292.68	250.43	179.48	186.11	186.11

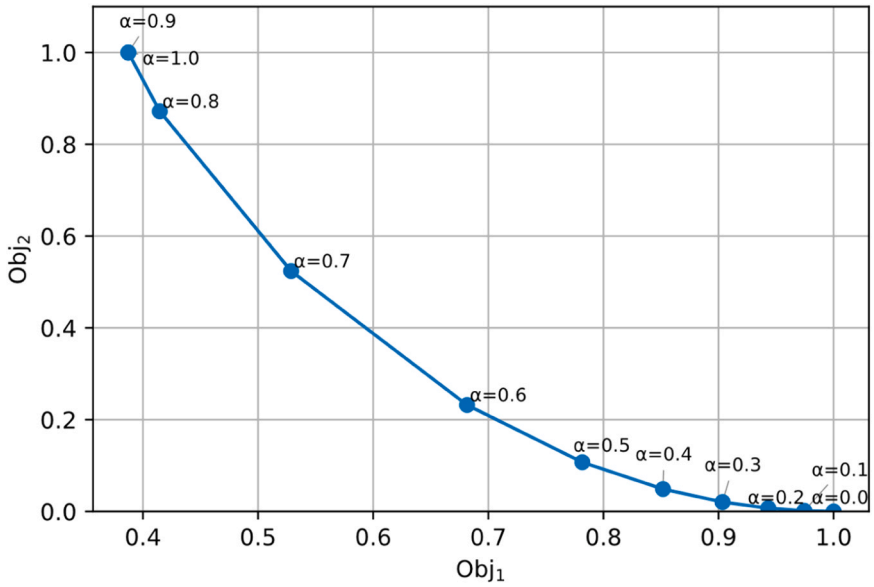

Fig. 7. WSCC 9-bus network – Pareto front.

calculated with the two approaches, equal to 0.098 %, highlights the effectiveness of the proposed method for post-fault voltage estimation.

The voltage responses of the inverters are reported in Fig. 9. It can be observed that the IBR connected to node 38 operates in grid-forming mode, while for the IBR connected to node 39, the current control under fault conditions is activated.

On the other hand, Table 9 shows the comparison between the analytical procedure results and the ones obtained using standard procedures for calculating voltages under SC conditions. It is evident that these procedures are unsuitable when the IBRs in the network are controlled according to the Italian grid code.

Moreover, to provide a broader validation, a 3 phases symmetrical fault has been applied at each of the network buses and the resulting voltages' profile has been analyzed both with the proposed approach and with the complete Power Factory simulation. Fig. 10 shows the maximum percentage error (i.e. the maximum percentage difference in the voltage amplitude among all the network nodes) as a function of the selected fault location. The results prove the reliability of the developed procedure in evaluating nodal voltages. Indeed, the largest error, obtained when the fault location is at node 20, is of 0.098 %, as previously analysed.

Finally, the optimization problem was solved for considering the fault at bus 20 and the additional susceptances, as dictated by the method, were inserted in the PowerFactory network. Their values and the voltages at the generation nodes are presented in Table 10. It is observed that the optimization strategy is effective and that, as before, it is reasonable that, with the aim of minimizing the reactive power injections, some voltages are kept at their minimum admissible value, i.e. 0.85.

In order to analyse the trade-off between minimisation of the reactive power injection at strategic nodes and the voltage drop at those nodes, a Pareto analysis has been developed, varying the coefficient α between 0 and 1 with a step of 0.1. To this purpose, the reference voltages $V_{ref,i}$ for strategic nodes have been considered equal to the rated voltage (i.e., $V_{ref,i} = 1$). The voltage modules at strategic nodes when varying α are reported in Table 11, while nodal reactive power injections at strategic nodes are reported in Table 12.

Differently from the WSCC case study, considering α= 0, it is not possible to keep all the voltages at the strategic nodes at the rated value. On the other hand, similarly to WSCC case study, when prioritizing just the minimization of the nodal reactive power injections some nodal voltage reach the minimum allowable value of 0.85 [p.u.]. In this latter scenario, a reduction of −40 % of reactive power injection is reached, with respect to the one in the scenario with α= 0.

The trade-off between the two objectives is well represented by the Pareto front shown in Fig. 11, in which Obj_1 and Obj_2 are respectively the first and second term of (27). It is evident that for low values of α, it is possible to reduce the overall nodal reactive power injection while keeping the nodal voltages close to the rated values. On the other hand, increasing α beyond 0.3, the reduction in Obj_1 is counterbalanced by a sharp increase of Obj_2.

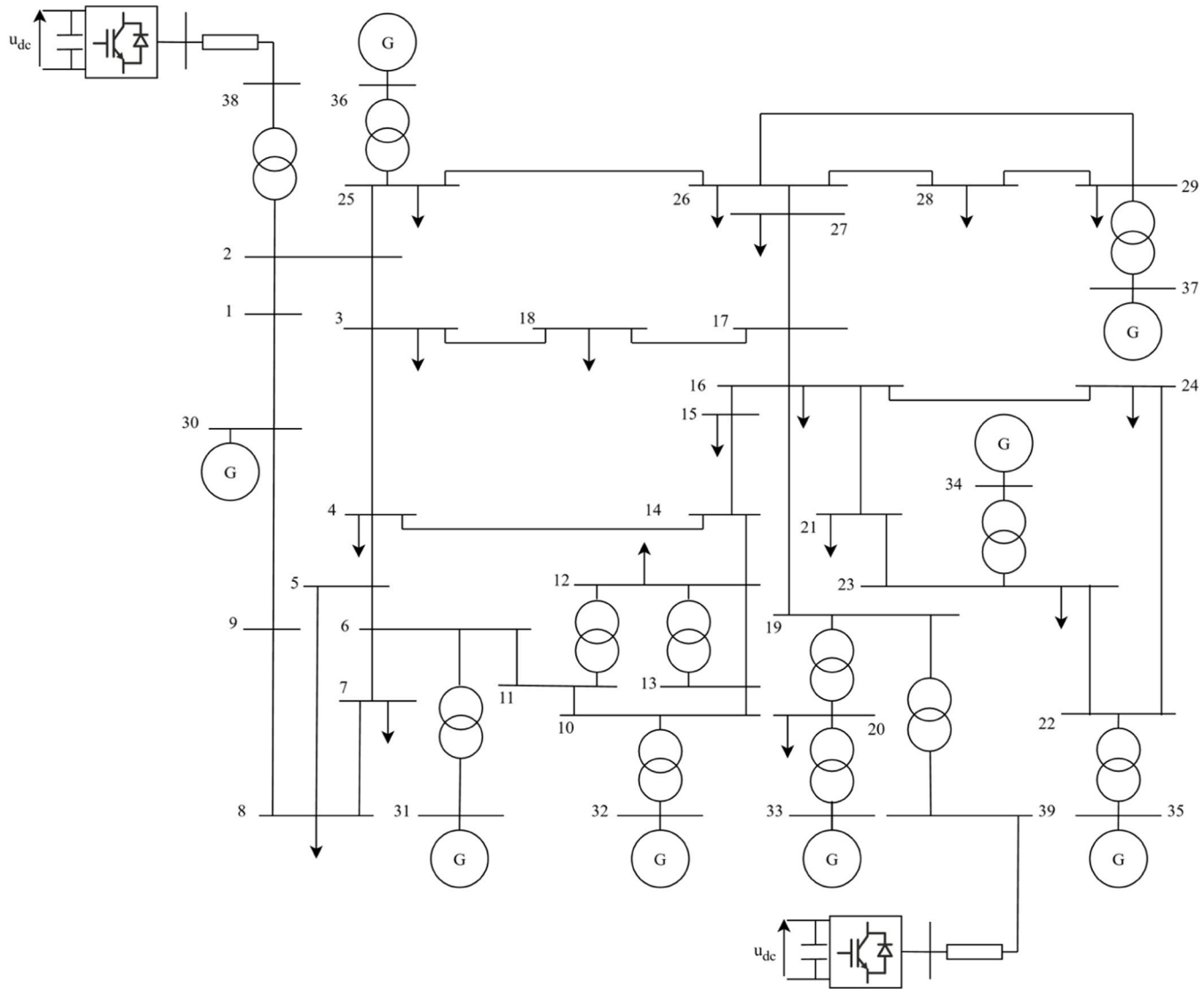

Fig. 8. IEEE 39-Bus Network implemented in DIgSILENT PowerFactory.

Table 7
IEEE 39-bus network – Load Flow assignments.

	Active power [MW]	Voltage [p.u]
Bus 30	1000.0	1.0300
Bus 31 (Slack)	-	0.9820
Bus 32	650.0	0.9831
Bus 33	508.0	1.0123
Bus 34	650.0	1.0493
Bus 35	560.0	1.0635
Bus 36	540.0	1.0278
Bus 37	830.0	1.0265
Bus 38	30.0	1.0000
Bus 39	30.0	1.0000

Table 8
IEEE 39-bus network – Post-fault voltages.

Solutions	Proposed method	Reference	Module deviation
$\dot{V}_{30}$	$1.0260\angle 15.68°$	$1.0259\angle 15.68°$	−0.009 %
$\dot{V}_{31}$	$0.9397\angle 1.33°$	$0.9395\angle 1.33°$	−0.021 %
$\dot{V}_{32}$	$0.9358\angle 7.87°$	$0.9355\angle 7.87°$	−0.032 %
$\dot{V}_{33}$	$0.2445\angle 15.68°$	$0.2440\angle 15.64°$	−0.20 %
$\dot{V}_{34}$	$0.9497\angle 6.62°$	$0.9488\angle 6.64°$	−0.095 %
$\dot{V}_{35}$	$0.9854\angle 9.05°$	$0.9848\angle 9.07°$	−0.061 %
$\dot{V}_{36}$	$0.9854\angle 8.21°$	$0.9851\angle 8.22°$	−0.030 %
$\dot{V}_{37}$	$0.9955\angle 11.58°$	$0.9953\angle 11.59°$	−0.020 %
$\dot{V}_{38}$	$0.9371\angle 1.47°$	$0.9367\angle 1.47°$	−0.042 %
$\dot{V}_{39}$	$0.3055\angle -2.83°$	$0.3052\angle -2.92°$	−0.098 %

4. Discussion

In this section a discussion on the proposed methodology its relevant results is provided. First of all, it is important to highlight that the proposed semi-analytical procedure developed in Section 2.2 is general: in the present paper, it has been implemented considering the post-fault voltage support actions required by the Italian TSO to IBRs, described in Attachment A.79 [20] to the grid code for BESSs, as reported and discussed in Section 2.1. The semi-analytical procedure can be easily applied to be compliant with all the other national regulatory frameworks provided that the relation between the phasor of the injected current at the IBR bus and the corresponding bus voltage phasor is either linear or effectively approximated with a linear one. For example, the United Kingdom Grid Code [34] has a provision similar to the one of the Italian TSO, asking for reactive current injection proportional to the voltage drop, not providing strict requirements on during-fault active current injection.

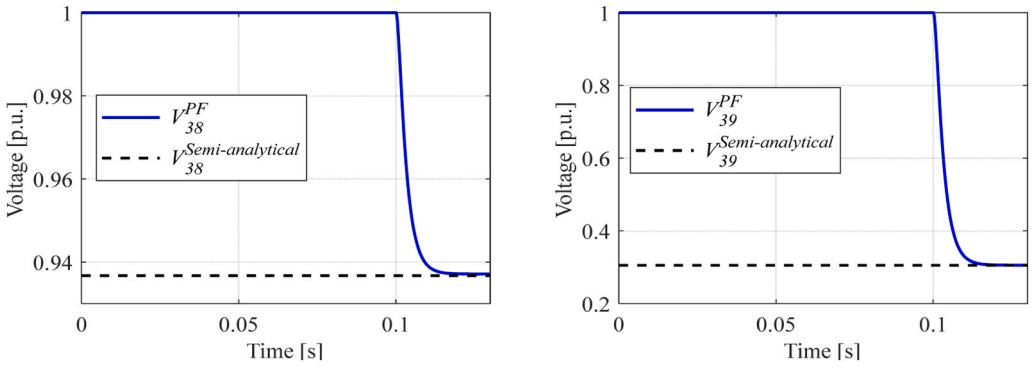

Fig. 9. Voltage magnitude of IBRs connected to nodes 38 and 39.

Table 9
IEEE 39-bus network – Post-fault voltages – Comparison with other standards.

Solutions	Proposed method	VDE 0102	IEC 60909	ANSI	Complete
V_{30}	1.0260	1.0927	1.0927	0.9819	1.0199
V_{31}	0.9397	1.0371	1.0371	0.9325	0.9151
V_{32}	0.9358	1.0285	1.0285	0.9249	0.9100
V_{33}	0.2445	0.3857	0.3857	0.3509	0.3153
V_{34}	0.9497	0.9682	0.9682	0.8713	0.9120
V_{35}	0.9854	0.9943	0.9943	0.8944	0.9523
V_{36}	0.9854	1.0305	1.0305	0.9269	0.9576
V_{37}	0.9955	1.0509	1.0509	0.9448	0.9671
V_{38}	0.9371	0.9620	0.9620	0.8674	0.8798
V_{39}	0.3055	0.3020	0.3020	0.2850	0.2868

The aim of the optimization problem presented in Section 2.3 is to assess the share of additional voltage supporting resources to be installed at a set of nodes considered strategic (i.e., whose voltage should not undergo a considerable drop even during faults). A multi-objective approach has been adopted, providing a Pareto front analysis, showing the trade-off between the minimization of the reactive power circulation and the support of voltage at values close to the rated one. From a modelling point of view, the NLP model can be easily extended up to a real-transmission network scale: indeed, the mathematical formulation is completely general. The main drawbacks of the NLP are that the existence and the uniqueness of the optimal solution cannot be demonstrated and that the computational power required to solve a large-scale problem may be considerable: to these purposes, a linearization of the NLP problem may be taken into account.

Both the proposed methodologies have been tested and validated through DIgSILENT PowerFactory simulations, in which full-control of IBRs has been implemented: the simulations acknowledged the validity of the approaches on the WSCC 9-bus and New England 39-bus test cases.

Further analyses will be performed to validate the model on more complex networks, with the aim of assessing the computational scalability of the models. In addition, as will be highlighted in the Conclusions section, the implementation of statistical and sensitivity analyses would enhance the applicability of this research, in order to provide the TSOs with dedicated tools for the assessment of the voltage support needs of the network during SC faults.

5. Conclusions

This paper presented a comprehensive methodology to face the

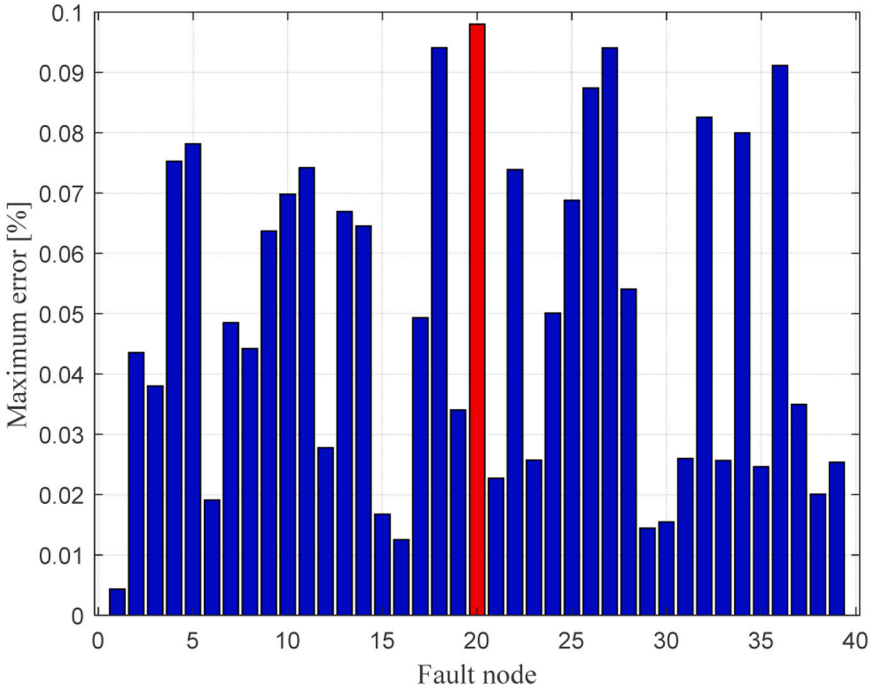

Fig. 10. IEEE 39-bus network – Maximum percentage error as function of the fault node.

Table 10
IEEE 39-bus network – Optimization results.

Bus	Q_{add} [MVAR]	B_{add} [S]	$\dot{V}$	
			Proposed method	Reference
30	0	0	1.0272∠15.62	1.0268∠15.611
31	0	0	0.9531∠0.8741	0.9525∠0.8732
32	3.64	18.49	0.9507∠7.2748	0.9502∠7.2747
33	0	0	0.8500∠3.7980	0.8503∠3.7980
34	0	0	0.9810∠5.6539	0.9814∠5.6538
35	0	0	1.0099∠8.2415	1.0091∠8.2413
36	0	0	0.9987∠7.7129	0.9982∠7.7121
37	0	0	1.005∠11.1265	1.0048∠11.1261
38	0	0	0.9569∠0.8389	0.9566∠0.8381
39	1.71	5.88	0.8500∠-9.0016	0.8500∠-9.0009

problem of faults in transmission networks with high penetration of IBRs. Such methodology consists of a quasi-analytical approach for calculating post-fault nodal voltages and an optimization problem to determine the amount of reactive power to be supplied at specific network nodes to restore nodal voltages to acceptable levels. In this approach, IBRs are modeled in compliance with the prescriptions of the Italian grid code. However, the methodology can be easily adapted to align with the requirements of other transmission system operators.

The proposed approach was tested on the IEEE 9-bus and 39-bus systems, both appropriately modified to include IBRs, and validated through RMS simulations carried out in the DIgSILENT PowerFactory environment that implemented all the network components with a much higher level of detail. An excellent agreement was found both in the post fault voltage evaluation and in the voltage support thanks to the optimal susceptance connection. Moreover, the limitations of conventional standards in accurately capturing the behaviour required of IBRs under fault conditions, as specified by the Italian grid code, were analysed.

The main contribution of this study lies in the definition of a semi-analytical framework for assessing nodal voltages during faults, which requires only basic numerical operations and, therefore, overcomes the dependency on dedicated power system software, and in the introduction of an optimization strategy to determine the necessary reactive power to sustain voltage. The combination of these two strategies provides a practical and flexible tool for TSOs, enabling them to evaluate network behaviour under fault conditions and to plan suitable supporting resources in systems dominated by IBRs. By this approach, the proposed tool addresses a relevant research gap by delivering a short-circuit calculation method that better reflects TSO requirements while avoiding reliance on numerical solvers and dedicated software. Extending existing procedures that are limited to post-fault voltage assessment, it also provides a systematic framework to help TSOs quantify the additional resources needed to ensure adequate voltage support at strategic network nodes.

Future work will be related to the identification of the most suitable technologies and the fault nodes to which they should be connected. Additionally, statistical and sensitivity analyses will be necessary to provide the TSO with an adequate tool for defining the necessary network upgrades and installations in a scenario characterized by a high penetration of IBRs. By integrating the proposed methodology, TSOs will be able to plan investments, optimize the use of reactive power resources and ensure operation that is consistent with network code requirements under fault conditions.

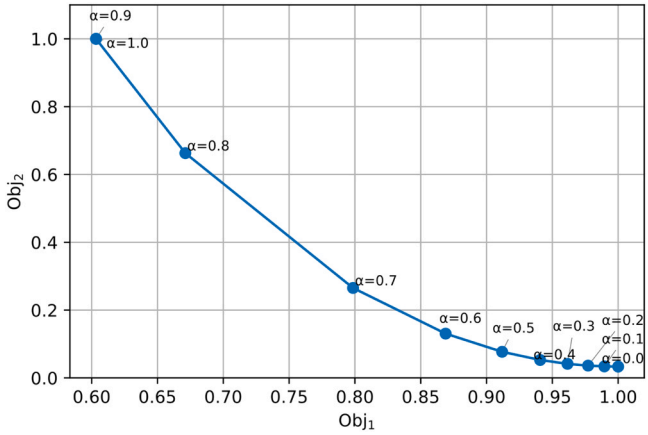

Fig. 11. IEEE 39-bus network – Pareto front.

Table 11
IEEE 39-bus network – Pareto analysis of nodal voltages.

	$\alpha = 0$	$\alpha = 0.1$	$\alpha = 0.2$	$\alpha = 0.3$	$\alpha = 0.4$	$\alpha = 0.5$	$\alpha = 0.6$	$\alpha = 0.7$	$\alpha = 0.8$	$\alpha = 0.9$	$\alpha = 1$
Bus 30	1.029	1.029	1.029	1.029	1.029	1.028	1.028	1.028	1.027	1.027	1.027
Bus 31	0.999	0.998	0.996	0.994	0.991	0.987	0.980	0.970	0.954	0.953	0.953
Bus 32	0.999	0.997	0.995	0.993	0.990	0.985	0.978	0.967	0.952	0.951	0.951
Bus 33	1.000	0.996	0.992	0.986	0.978	0.967	0.951	0.923	0.865	0.850	0.850
Bus 34	0.995	0.993	0.992	0.992	0.992	0.991	0.990	0.988	0.984	0.981	0.981
Bus 35	1.020	1.019	1.019	1.019	1.018	1.018	1.017	1.015	1.013	1.010	1.010
Bus 36	1.011	1.010	1.010	1.010	1.009	1.008	1.006	1.004	1.000	0.999	0.999
Bus 37	1.011	1.011	1.011	1.010	1.010	1.010	1.009	1.008	1.006	1.005	1.005
Bus 38	0.996	0.995	0.994	0.992	0.989	0.986	0.980	0.972	0.959	0.957	0.957
Bus 39	0.999	0.997	0.994	0.990	0.984	0.977	0.966	0.947	0.909	0.850	0.850

Table 12
IEEE 39-bus network – Pareto analysis of nodal reactive power injections.

	$\alpha = 0$	$\alpha = 0.1$	$\alpha = 0.2$	$\alpha = 0.3$	$\alpha = 0.4$	$\alpha = 0.5$	$\alpha = 0.6$	$\alpha = 0.7$	$\alpha = 0.8$	$\alpha = 0.9$	$\alpha = 1$
Bus 30	0.01	0.01	0.01	0.01	0.00	0.00	0.00	0.00	0.00	0.00	0.00
Bus 31	204.83	198.45	190.16	179.46	165.29	145.65	116.62	69.37	0.03	0.00	0.00
Bus 32	246.27	238.11	227.35	213.44	195.07	169.66	132.23	71.67	0.02	0.00	0.00
Bus 33	5340.45	5295.94	5240.39	5169.14	5074.42	4942.40	4745.67	4421.52	3789.00	3636.26	3636.26
Bus 34	10.58	1.92	0.04	0.02	0.00	0.00	0.01	0.00	0.00	0.00	0.00
Bus 35	0.00	0.00	0.00	0.00	0.00	0.00	0.00	0.00	0.00	0.00	0.00
Bus 36	0.00	0.00	0.00	0.00	0.00	0.00	0.00	0.00	0.00	0.00	0.00
Bus 37	0.00	0.00	0.00	0.00	0.00	0.00	0.00	0.00	0.00	0.00	0.00
Bus 38	146.55	142.17	136.14	128.26	117.83	103.35	81.90	46.89	0.02	0.00	0.00
Bus 39	2898.25	2877.71	2850.84	2816.09	2770.00	2705.95	2610.93	2455.51	2148.96	1701.33	1701.33

CRediT authorship contribution statement

Matteo Fresia: Writing – original draft, Validation, Software, Methodology, Investigation, Data curation, Conceptualization. **Manuela Minetti:** Writing – original draft, Validation, Software, Methodology, Investigation, Data curation, Conceptualization. **Andrea Bonfiglio:** Writing – review & editing, Validation, Supervision, Methodology, Formal analysis. **Renato Procopio:** Writing – review & editing, Validation, Supervision, Methodology, Formal analysis, Conceptualization.

Declaration of Competing Interest

The authors declare that they have no known competing financial interests or personal relationships that could have appeared to influence the work reported in this paper.

Data availability

Data will be made available on request.

References

[1] L. Michi, et al., The effects of new 2030 scenario: reduction of short-circuit power and widening of voltage dips, 2018 AEIT Int. Annu. Conf. (2018) 1–6.
[2] E. Marrazi, G. Yang, P. Weinreich-Jensen, Allocation of synchronous condensers for restoration of system short-circuit power, J. Mod. Power Syst. Clean. Energy 6 (1) (2018) 17–26.
[3] R. Marconato, Steady State Behavior Controls, Short Circuits and Protection Systems (Electric Power Systems). 2004.
[4] N. Baeckeland, D. Chatterjee, M. Lu, B. Johnson, G.S. Seo, Overcurrent limiting in grid-forming inverters: a comprehensive review and discussion, IEEE Trans. Power Electron. 39 (11) (2024) 14493–14517.
[5] IEC 60909 Series: Short-circuit Currents in Three-Phase AC Systems, 2001.
[6] J. Song, M. Cheah-Mane, E. Prieto-Araujo, O. Gomis-Bellmunt, On the solution of equilibrium points of power systems with penetration of power electronics considering converter limitation, IEEE Access 9 (2021) 67143–67153.
[7] J. Song, M. Cheah-Mane, E. Prieto-Araujo, O. Gomis-Bellmunt, Short-circuit analysis of AC distribution systems dominated by voltage source converters considering converter limitations, IEEE Trans. Smart Grid 13 (5) (2022) 3867–3878.
[8] J. Song, M. Cheah-Mane, E. Prieto-Araujo, O. Gomis-Bellmunt, Short-circuit analysis of grid-connected PV power plants considering inverter limits and grid-support, 11th Sol. Storage Power Syst. Integr. Workshop (SIW 2021) 2021 (2021) 154–160.
[9] J. Song, M. Cheah-Mane, E. Prieto-Araujo, O. Gomis-Bellmunt, Short-circuit analysis of grid-connected PV power plants considering inverter limits, Int. J. Electr. Power Energy Syst. 149 (2023) 109045.
[10] J. Song, et al., A short-circuit calculation solver for power systems with power electronics converters, Int. J. Electr. Power Energy Syst. 157 (2024) 109839.
[11] I. Kim, Steady-state short-circuit current calculation for internally limited inverter-based distributed generation sources connected as current sources using the sequence method, Int. Trans. Electr. Energy Syst. 29 (12) (2019) e12125.
[12] R.M. Furlaneto, I. Kocar, A. Grilo-Pavani, U. Karaagac, A. Haddadi, E. Farantatos, Short circuit network equivalents of systems with inverter-based resources, Electr. Power Syst. Res. 199 (2021) 107314.
[13] M. Patel, Opportunities for standardizing response, modeling and analysis of inverter-based resources for short circuit studies, IEEE Trans. Power Deliv. 36 (4) (2021) 2408–2415.
[14] A. Rajapakse, R. Majumder, S.G.R. Energy, R. Nelson, Modification of commercial fault calculation programs for wind turbine generators, IEEE Power Energy Soc. 81 (2020).
[15] I. Kim, A calculation method for the short-circuit current contribution of current-control inverter-based distributed generation sources at balanced conditions, Electr. Power Syst. Res. 190 (2021) 106839.
[16] Z. Wang, L. Hao, L. Wang, J. He, Analysis and general calculation of DC fault currents in MMC-MTDC grids, Electr. Power Syst. Res. 224 (2023) 109709.
[17] T. Li, Y. Li, Y. Zhu, N. Liu, X. Chen, DC fault current approximation and fault clearing methods for hybrid LCC-VSC HVDC networks, Int. J. Electr. Power Energy Syst. 143 (2022) 108467.
[18] S. Yuan, J. Yan, Y. Yu, C. Zhao, G. Su, X. Li, Calculation method of short-circuit fault current in flexible DC grid, Energy Rep. 8 (2022) 461–468.
[19] J. Wang, et al., Open-source short-circuit current solver for power systems with renewable energy sources and HVDC links, Int. J. Electr. Power Energy Syst. 167 (2025) 110651.
[20] TERNA, Impianti con sistemi di accumulo elettrochimico: Condizioni generali di connessione alle reti AAT e AT - Sistemi di protezione regolazione e controllo, 2023.
[21] P.M. Anderson, A.A. Fouad, Power System Control and Stability, John Wiley & Sons, 2008.
[22] J. Venkateswaran, P. Manohar, K. Vinothini, B.T.M. Shree, R. Jayabarathi, Contingency analysis of an IEEE 30 bus system, 2018 3rd IEEE Int. Conf. Recent Trends Electron. Inf. Commun. Technol. (RTEICT) (2018) 328–333.
[23] IEEE Standard for Interconnection and Interoperability of Distributed Energy Resources with Associated Electric Power Systems Interfaces, IEEE Std 15472018 (Revis. IEEE Std 15472003 (2018) 1–138.
[24] J. Rocabert, A. Luna, F. Blaabjerg, P. Rodriguez, Control of power converters in AC microgrids, IEEE Trans. Power Electron. 27 (11) (2012) 4734–4749.
[25] P. Kundur, Power System Stability. 2007, pp. 7-1.
[26] Nine-bus System. Heinrich-Hertz-Str9, 72810 Gomaringen, Germany: DIgSILENT GmbH, 2016.
[27] M.A. Pai, Energy Function Analysis for Power System Stability, Springer US, 2012.
[28] J. Lofberg, YALMIP: a toolbox for modeling and optimization in MATLAB. 2004 IEEE International Conference on Robotics and Automation (IEEE Cat. No.04CH37508), 2004, pp. 284–289.
[29] A. Wächter, L.T. Biegler, On the implementation of an interior-point filter line-search algorithm for large-scale nonlinear programming, Math. Program. 106 (1) (2006) 25–57.
[30] *DIgSILENT Power*Factory 2016: Technical Reference Documentation Synchronous Machine (Version 2016). Heinrich-Hertz-Str9, 72810 Gomaringen, Germany, 2016.
[31] P.W. Sauer, M.A. Pai, Power System Dynamics and Stability, Prentice Hall, 1998.
[32] T.B. Nguyen, M.A. Pai, Dynamic security-constrained rescheduling of power systems using trajectory sensitivities, IEEE Trans. Power Syst. 18 (2) (2003) 848–854.
[33] J. Das. Short-Circuits in AC and DC Systems: ANSI, IEEE, and IEC Standards, CRC Press, 2017.
[34] National Energy System Operator, "The Grid Code," 2025.